Applied Surface Science 297 (2014) 75–83

Contents lists available at ScienceDirect

Applied Surface Science

journal homepage: www.elsevier.com/locate/apsusc

Oxidation of Ag nanoparticles in aqueous media: Effect of particle size and capping

Yuri L. Mikhlin[a,*], Elena A. Vishnyakova[a,b], Alexander S. Romanchenko[a], Svetlana V. Saikova[b], Maxim N. Likhatski[a], Yurii V. Larichev[c], Fedor V. Tuzikov[c], Vladimir I. Zaikovskii[c], Sergey M. Zharkov[b,d]

[a] Institute of Chemistry and Chemical Technology of the Siberian Branch of the Russian Academy of sciences, Akademgorodok 50/24, Krasnoyarsk 660036, Russia
[b] Siberian Federal University, Svobodny pr. 79, Krasnoyarsk 660041, Russia
[c] Boreskov Institute of Catalysis of the Siberian Branch of the Russian Academy of sciences, Lavrent'ev av., 5, Novosibirsk 630090, Russia
[d] Kirensky Institute of Physics of the Siberian Branch of the Russian Academy of sciences, Akademgorodok 50/38, Krasnoyarsk 660036, Russia

ARTICLE INFO

Article history:
Received 1 October 2013
Accepted 14 January 2014
Available online 27 January 2014

Keywords:
Silver nanoparticles
Oxidation
Resistive switching effect
X-ray photoelectron spectroscopy

ABSTRACT

Many applications and environmental impact of silver-bearing nanomaterials critically depend upon their specific reactivity, which is still poorly understood. Here, silver nanoparticles (Ag NPs) of about 3–5 nm and 10–12 nm in diameter, uncapped and capped with L-glucose or citrate, were prepared, characterized using UV–vis absorption spectroscopy, SAXS, TEM, and their (electro)chemical oxidation was examined in comparison with each other and bulk metal applying scanning tunneling microscopy and spectroscopy, cyclic voltammetry, and XPS. A resistive switching effect was found in the tunneling spectra measured in air at the smaller uncapped Ag NPs deposited on HOPG and was interpreted in terms of Ag transfer between the particle and the probe. The anodic oxidation of these Ag NPs in 1 M NaOH yielded 3D Ag_2O, while only a layer of "primary" Ag(I) oxide emerged on larger uncapped nanoparticles during the potential sweep. The formation of AgO at higher potentials proceeded readily at the "primary" oxide but was retarded at the smaller NPs. The citrate- and glucose-capping substantially impeded the formation both of Ag_2O and AgO. The findings highlighted, particularly, a non-trivial effect of particle size and transient mobilization of Ag species on the reactions of silver nanoparticles.

1. Introduction

Silver nanoparticles have attracted a great deal of attention owing their applications in catalysis, sensors, electronics, biomedicine and other fields [1–5], which are based on specific properties of nanoparticles and depend upon their size, shape, stabilizing agents, aggregation, support, and so on. The oxidation of Ag NPs in aqueous media affording silver oxides or dissolved metal ions is also of considerable fundamental and practical interest for understanding the biological activity and environmental impacts of nanosilver [6–9]. The O and Ag species on Ag NPs have been widely explored in relation to catalysis using X-ray and UV photoelectron spectroscopy and other surface science techniques [10–14], mainly at low oxygen pressure. The recent studies have employed synchrotron based near ambient pressure methods; in particular, Rocha et al. [14] have identified five atomic oxygen species in mbar pressure range and temperatures up to 600 °C. Nevertheless, the complex dynamic processes are far from being completely understood even in the model systems.

The anodic oxidation of bulk silver has been extensively studied in alkaline solutions applying electrochemical, spectroscopic and microscopic techniques [15–21]. The reaction is commonly accepted to proceed in several stages involving underpotential adsorption of OH^- and then atomic oxygen species [18], the formation of a monolayer of Ag(I) oxide or hydroxide, thin layer of irregular "primary" Ag_2O or undersurface atomic oxygen and then 3D Ag_2O having cuprite structure, with some amount of Ag dissolving during the initial stages. Silver(II) oxide AgO (in fact, $Ag^+Ag^{3+}O_{2-x}$) arises from Ag_2O phase at the solid-electrolyte interface at higher potentials [16], with oxygen deficiency and a fraction of Ag^{3+} depending on the electrode potential and oxidation time [19,21]. The electrochemical oxidation of metal nanoparticles has been studied in few works [22–27]. In particular, Ng et al. [24] have observed enhanced stability of Ag clusters having a diameter of 0.3–0.6 nm. Ivanova and Zamborini [25] have reported that the peak potential for oxidation of Ag^0 to Ag shifts positive as the

* Corresponding author.
E-mail addresses: yumikh@icct.ru, yumikh@mail.ru (Y.L. Mikhlin).

0169-4332/$ – see front matter © 2014 Elsevier B.V. All rights reserved.
http://dx.doi.org/10.1016/j.apsusc.2014.01.081

citrate-capped Ag NP diameter increases in the range 8–50 nm, in line with the thermodynamic potential shift. A reversible oxidation of about 4.5 nm adenosine triphosphate capped Ag NPs (forming a single-layer film on a gold electrode) to silver halide NPs in aqueous halide solutions and to Ag_2O NPs in hydroxide solutions has been suggested to occur via a redox-driven solid-state phase transformation, indicating complete oxidation and reduction of all Ag atoms in each NP [26,27].

Although the behavior in the aqueous environment of Ag NPs manufactured using various synthetic protocols have been documented by many authors (see [6–8,28–40] and references herein), experimental data regarding the effect of size, shape, capping, etc., on the wet chemical oxidation and dissolution of colloidal and supported Ag NPs are still fragmentary. For example, Ma and coworkers [38] have reported that solubility of Ag NPs ranging from 5 to 80 nm in diameter in 1 mM $NaHCO_3$ (pH 8) increases for smaller particles but much less depends on polymer coating type and synthesis method. Liu and Hurt (2010) have found that dissolution of 1.5–7 nm citrate-stabilized nanosilver colloids decreases with increasing pH or addition of humic or fulvic acids, while sea salts have only a minor effect. Sotiriou et al. [39] have revealed that only one to two surface silver oxide monolayers at Ag NPs of 4–9 nm in diameter (without any protecting agents) supported on nanostructured silica dissolve in water; when the oxide layers are removed, Ag^+ ion leaching and its antibacterial activity drastically decreases. It is noteworthy that dissolved oxygen causes dissolution and re-crystallization of nanoparticles already during their synthesis [40,41]; researchers have pointed out a role of solubilised Ag^+ in transformations of Ag nanoparticles [37,39,41–43]. In general, however, specific mechanisms of the reactions are still insufficiently understood.

The aim of the current work was to study the behavior of Ag NPs prepared by several different methods in aqueous media and to gain insight into the reaction mechanisms involved, with emphasis on the oxidation of nanoparticles simply deposited on an inert substrate. We report here that the size and capping shell influence the reactions of Ag NPs, which do not form a continuous film on highly-oriented pyrolytic graphite (HOPG), in a rather complicated manner, with intermediary mobile Ag species playing an important role in the oxidation pathway.

2. Experimental

2.1. Materials and synthetic procedures

Four types of silver nanoparticles without (uncapped, or "naked") and with stabilizing coatings were synthesized using simple procedures previously described in the literature [41,43,44] and somewhat modified here. All chemicals were analytical grade and used without further purification; double or triple distilled water was used throughout the experiments. Three types of Ag NPs were prepared via reduction of silver nitrate solution with sodium borohydride. Uncapped Ag NPs having a nominal diameter of about 12 nm or a bimodal size distribution with mean diameters of about 3 nm and 10 nm (see below for detail) were manufactured using the initial molar ratios $AgNO_3$ to $NaBH_4$ of 1 and 10, respectively. In typical experiments, 0.5 ml of fresh ice-cooled 20 mM or 2 mM sodium borohydride was added with vigorous agitation to 1 mM $AgNO_3$ solution (10 ml) kept in a glass flask. The colloidal solutions were stable for about 2 h; UV–vis spectra, SAXS patterns were measured and deposition experiments were conducted in several minutes after mixing the reactants. To produce about 12 nm Ag NPs with citrate as a capping agent, 1 ml of trisodium citrate solution (34 mM) was added to 0.5 ml of 20 mM $AgNO_3$, the mixture was diluted under agitation with 98 ml of water followed by injection of 0.5 ml of 20 mM $NaBH_4$, so the molar ratio of the $AgNO_3$: Na_3cit: $NaBH_4$ reactants was 1:3:1. The Ag NPs with a diameter of 2–5 nm stabilized with glucose molecules were prepared via addition of 50 mM L-glucose solution (10 ml) to 2 mM $AgNO_3$ (10 ml) and boiling the reaction media at the water bath under microwave irradiation for 10 min. The two sols of capped Ag NPs were stable for several weeks at least; all the experiments were performed within first hours after their preparation.

Specimens for XPS, scanning probe microscopy and electrochemical experiments were prepared by drying a drop of as-prepared Ag NP sols on freshly renewed surface of HOPG in air, commonly followed by cautious rinsing with water.

2.2. Characterization of Ag NPs

The colloidal solutions were characterized using UV–vis absorption spectroscopy, SAXS and dynamic light scattering (DLS). The UV–vis spectra were recorded on Specol 1300 (Analytik Jena) spectrophotometer in the 300–850 nm range using 1 cm quartz cuvette. The DLS data were collected using 90Plus spectrometer (Brookhaven Inst.). Small-angle X-ray scattering patterns were acquired from the sols loaded in standard X-ray quartz capillaries (1.5 mm) with Kristalloflex-805 (Siemens) and S3-MICRO (Hecus) devices applying Cu K irradiation (λ = 0.154 nm). The SAXS patterns were corrected for X-ray absorption, collimation, and background scattering, particle size distribution functions were calculated for spherical nanoparticles using the indirect Fourier transform algorithm implemented in the optimization program [45].

JEM-2010 and JEM-2100 transmission electron microscopes (JEOL) operating at 200 kV were used for TEM and selected area electron diffraction (SAED) characterization of the products. Samples were prepared by placing a droplet of a colloidal solution on a carbon coated copper grid and allowing the solvent to evaporate at room temperature. The particle size distribution was estimated from micrographs for a minimum of 200 particles.

Tapping-mode atomic force microscopy (AFM) and scanning tunneling microscopy and spectroscopy (STM/STS) investigations were conducted in air (the relative humidity was about 60%) applying a multimode Solver P47 device equipped with a 14 mm scanner (NT-MDT, Russia). Silicon cantilevers with a typical force constant of 5 N m^{-1} (resonant frequencies of about 150 kHz) were employed in AFM. STM and STS measurements were made with a mechanically sharpened wire (90% Pt, 10% Ir) as a probe; positive voltage was defined as a positive potential on the sample with respect to the tip. The current vs voltage (*I–V*) curves were measured using a fixed tip-sample separation by breaking the feedback circuit for a 0.1 s. All curves represent reproducible measurements without changing the lateral position and the tip-sample distance.

X-ray photoelectron spectra and X-ray excited Ag MNN Auger spectra were taken with a SPECS instrument equipped with a PHOIBOS 150 MCD 9 hemispherical analyzer at electron take-off angle 90° with the pass energy of 8 eV for high-resolution spectra and 20 eV for survey spectra. The Mg Kα line (1253.6 eV) of a dual anode X-ray source was used for excitation. The pressure in an analytical chamber was in the range of 10^{-8} Pa. A low-energy electron flood gun was employed, when necessary, to eliminate inhomogeneous electrostatic charging of the samples. Sample etching with Ar^+ ions was performed using a scanning ion source operated at an accelerating voltage of 5 kV and Ar^+ emission current of 30 μA. The spectra were fitted using Gaussian–Lorentzian peak profiles after Shirley background subtraction with CasaXPS software.

Electrochemical experiments were carried out using HOPG plate with immobilized Ag NPs described above as a working electrode connected with a spring-loaded contact to a potentiostat P-30SM (Elins, Russia) in a three-department glass cell in atmosphere at 20 °C. The counter and reference electrodes were Pt wire

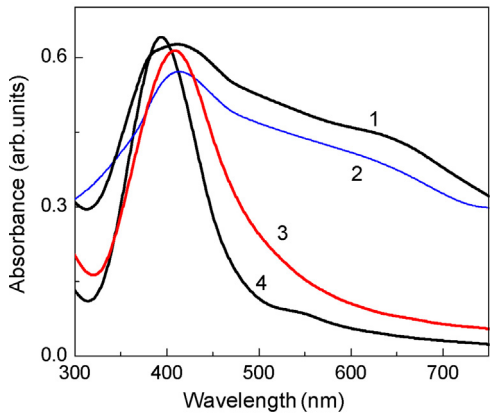

Fig. 1. UV–vis absorption spectra of silver hydrosols prepared using (1) $AgNO_3/NaBH_4 = 1$, (2) $AgNO_3/NaBH_4 = 10$, (3) $AgNO_3/Na_3cit/NaBH_4$, and (4) $AgNO_3$/glucose.

and saturated Ag/AgCl electrode, respectively; all potentials are given with respect to the latter. The reference electrode was placed in a separate compartment connected via a Luggin capillary in the main cell chamber through a closed wet ground-glass stopcock to prevent contamination of the electrolyte (1 M NaOH) by chloride-ions.

XPS, STM/STS, electrochemical experiments were repeated at least 5–6 times with the freshly prepared Ag NP colloidal solutions. The spectra, curves, etc., shown below are the most typical ones; although they may slightly vary (for example, photoelectron spectra having a spatial resolution less than 2 mm differ a little for various points on HOPG), the regularities reported here are fully reproducible.

3. Results and discussion

3.1. Characterization of synthesized silver nanoparticles

Fig. 1 represents UV–vis absorption spectra of four silver hydrosols afforded via different procedures. The solutions prepared using sodium borohydride without stabilizing molecules exhibit wide surface plasmon resonance (SPR) maxima at 410–420 nm and strong absorption at longer wavelengths, indicating considerable aggregation of Ag NPs [43]. This is consistent with DLS results showing that the apparent hydrodynamic diameter of the "naked" Ag NPs increases with time up to several hundred nm (not in figures). The UV–vis spectra of colloidal solutions obtained via citrate/borohydride- and glucose-assisted reactions have rather narrow SPR peaks centered at 400 nm and 390 nm, respectively, typical for capped Ag NPs [1].

TEM images reveal associated quasi-spherical nanoparticles with a mean diameter about 12 nm assembled in submicrometer structures with thinner nanobelts, possibly formed ex situ, in case of the $AgNO_3/NaBH_4 = 1$ product (Fig. 2a), while isolated particles of about the same size were manufactured when sodium citrate was

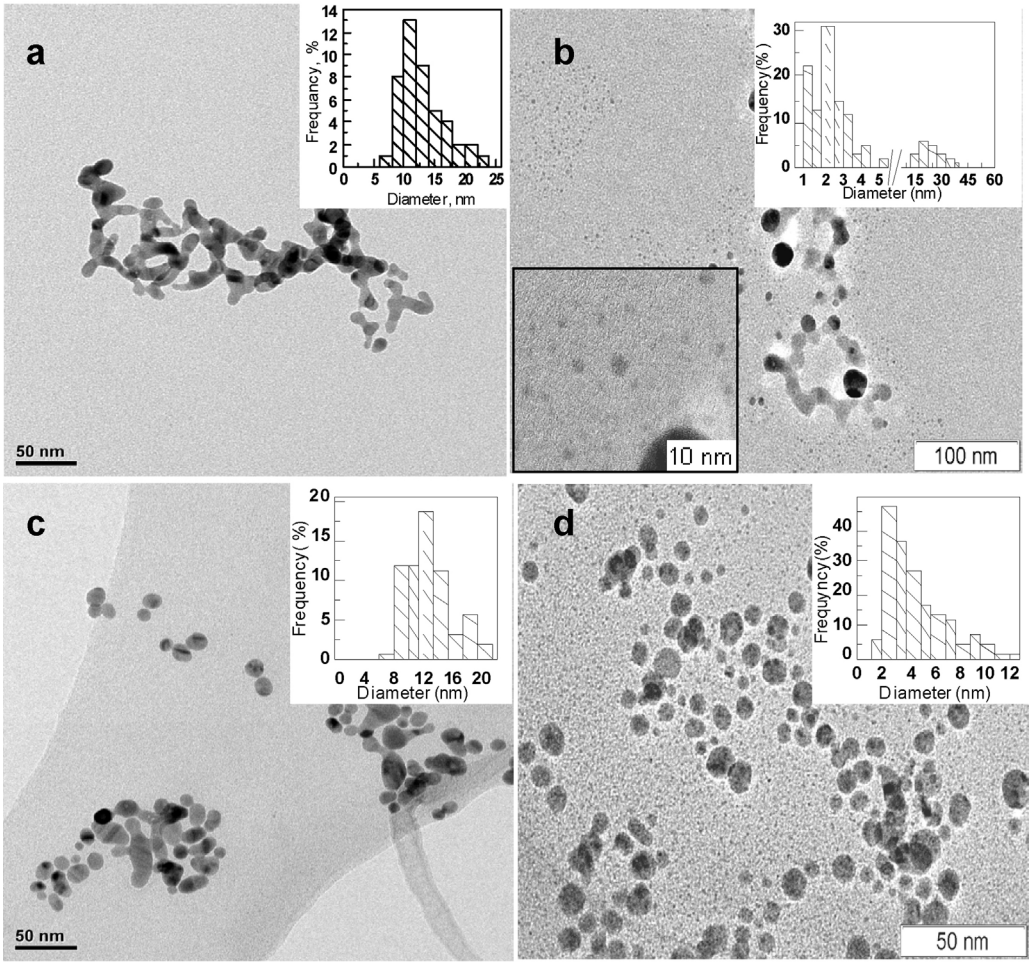

Fig. 2. Typical TEM micrographs and particle size distribution histograms for silver NPs prepared using (a) $AgNO_3/NaBH_4 = 1$, (b) $AgNO_3/NaBH_4 = 10$, (c) $AgNO_3/Na_3cit/NaBH_4$, and (d) $AgNO_3$/glucose.

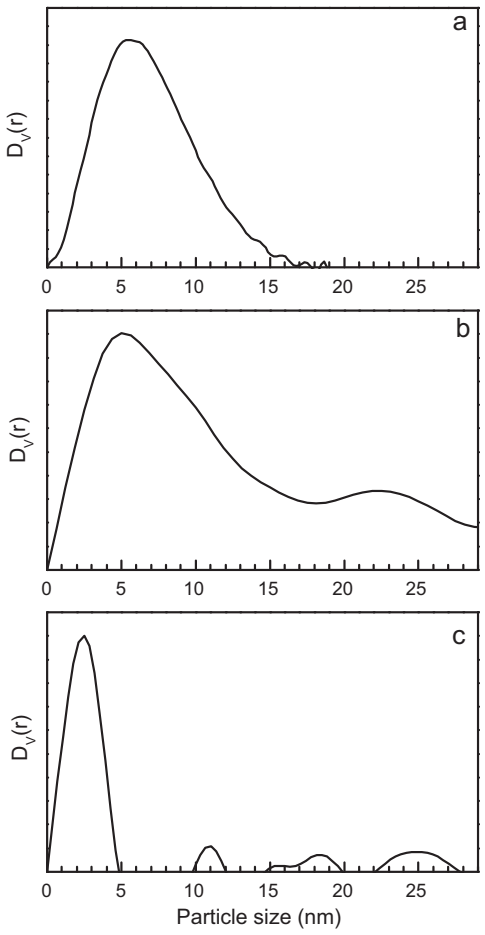

Fig. 3. Volume particle distribution functions derived from X-ray small-angle scattering for silver hydrosols prepared using (a) $AgNO_3/NaBH_4 = 1$, (b) $AgNO_3/NaBH_4 = 10$, (c) $AgNO_3$/glucose.

added as stabilizing agent (Fig. 2c). A big number of 2–5 nm clusters along with larger aggregated particles of 10–30 nm in diameter are seen in the TEM micrographs of the product obtained with a smaller concentration of the reducing agent ($AgNO_3/NaBH_4 = 10$) (Fig. 2b). In situ SAXS analysis (Fig. 3b) suggests that, in contrast to the higher content of borohydride, nanosilver in the solution comprises a fraction of the small particles. The formation of these tiny Ag NPs at a low concentration of $NaBH_4$ can be explained in terms of crystallization of Ag^0 clusters after partial dissolution of initially formed metal particles [41]; on the other hand, the larger particles may form via aggregation of the smaller ones. Although about 10 nm Ag NPs seemingly prevail in the volume, the smaller particles appear to determine the exposed surface area and so reactivity of the sample as it follows from their XPS and physicochemical properties described below. The glucose-assisted synthesis yields individual Ag NPs of 3–5 nm in diameter together with minor larger particles and their associates, although the size distribution functions determined from TEM images (Fig. 2d) and SAXS (Fig. 3c) are slightly different.

3.2. Supported Ag nanoparticles

3.2.1. Tunneling spectroscopy

HOPG was chosen as a support because of its chemical inertness, metallic electrical conductivity, atomic-scale smoothness and other properties suitable for electrochemical, AFM, STM/STS and XPS experiments; HOPG has been often used as a model substrate for metal nanoparticles including in catalysis [24,46–49]. STM and AFM images (Fig. 4 and Supplementary data) demonstrate that Ag NPs don't form a continuous film on HOPG but are largely arranged in associates up to 100 nm in size. At the same time, individual Ag NPs detected by TEM may be poorly seen due to insufficient resolution and/or brushing the nanoparticles away by a probe [46].

An interesting effect was observed in tunneling spectra of the uncapped Ag NPs prepared with $AgNO_3/NaBH_4 = 10$ and deposited on HOPG, where STM maps numerous 3–5 nm, some larger Ag NPs and their associates (Fig. 4a). The *I–V* curves acquired at the particles are typical for a material having metallic conductivity (Fig. 4b); similar curves were recorded at other types of Ag NPs prepared by different methods. After several measurement cycles, a surge in the current (restricted by the current cut-off of the amplifier) occurs at a small negative bias in the negative-going potential sweep after the positive one. As the number of cycles increases, sharp current changes arise also at positive biases (Fig. 4d). Such features are characteristic of resistive switching phenomena, which are now under intense scrutiny due to potential application in the next-generation non-volatile memory [50–52]. The switches consist of a metal oxide or a metal sulfide, including silver oxide [53], or organic molecules sandwiched between two metal electrodes, or two metal electrodes separated by approximately 10 nm with no material between the electrodes [54]. The resistance switching has been reported for arrays of Ag nanoparticles [55], however, at a voltage threshold much higher than in the current research.

The findings described above can be rationalized taking in mind that the current measured here is a sum of a tunneling current across the nanoparticle/Pt–Ir probe gap and faradic current through the water film occurring on the sample in atmosphere. We believe that some silver oxidizes and becomes mobile in the positive-going potential excursion, and then reduces and re-crystallizes at a negative bias at the Ag NP, decreasing the particle–probe distance or even making a contact between them (Fig. 4c,f,g). As the amount of mobilized silver grows, Ag atoms transfer from the nanoparticle to the probe, and a metal protrusion forms on the probe at a positive voltage (and so a negative potential at the probe) too (Fig. 4d,h,i). Nanocontacts may arise also within the Ag nanoparticle array, causing an abrupt drop in the resistance of the probe-Ag NPs-HOPG circuit. The phenomena are worthy of further investigation; at the moment, we would like to underline that the effect was found only for the smaller uncapped Ag nanoparticles, which, therefore, most easily release mobile Ag species, but not for other sorts of Ag NPs explored here (exhibiting only the curves shown in Fig. 4b).

3.2.2. X-ray photoelectron spectroscopy

The results of XPS analysis of the supported Ag NPs are shown in Fig. 5 (see also see also Electronic Supplementary material, Table 1) in comparison with the spectra of polished polycrystalline silver plate. The Ag $3d_{5/2,3/2}$ doublet spectra with the Ag $3d_{5/2}$ peak at binding energy (BE) of 368.3 ± 0.04 eV demonstrate that all the particles are composed preferentially of metallic silver [11–14,17–21]. Full width at half maximum (FWHM) of the Ag $3d_{5/2}$ bands, however, varies from 0.86 eV to 1.3 eV for different Ag NPs as a signature of some quantity of oxidized silver, which is minor for silver plate and bigger for Ag NPs, both uncapped and citrate-capped, and is higher for tiny Ag NPs prepared with lower concentration of borohydride and, most of all, with glucose. Auger Ag MNN spectra having the probing depth about 0.7 nm are more surface sensitive than Ag 3d lines (about 1.3 nm) [56], so Ag $M_4N_{45}N_{45}$ peaks shifted to lower kinetic energies from the value of 357.8 eV typical for elemental silver suggest that the oxidized Ag species occur mainly on the surface of smaller NPs. It should be reminded here that an increase in a positive charge localized at Ag atoms commonly results, in contrast to the majority of elements, in decreasing BE of Ag 3d lines and enhancing kinetic energies of the Auger band [10–14,17–19,21,34,49,57].

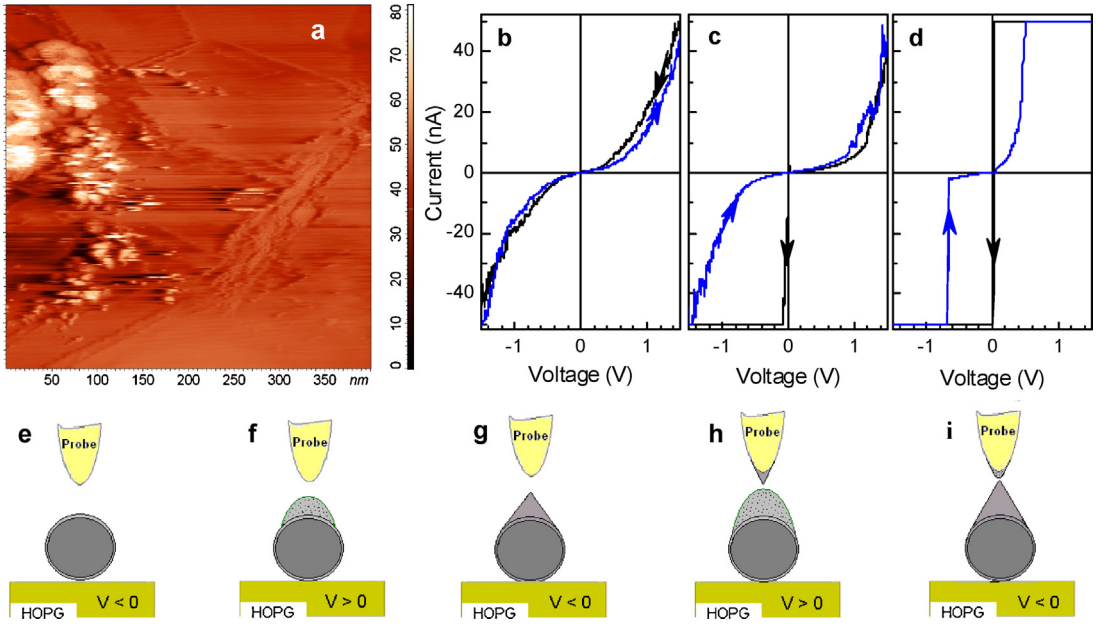

Fig. 4. Scanning tunneling microscopy image (I_{SP} = 0.5 nA, V_B = 0.3 V) of Ag NPs deposited on HOPG from the colloidal solution prepared with the molar ratio $AgNO_3/NaBH_4$ = 10 (a), typical *I*–*V* curves swept from −1.5 V to +1.5 V and back (b–d), and scheme explaining the resistive switching effect (e–i), see text for detail.

O 1s spectra (Fig. 5) contain strong bands from physically and chemically adsorbed water, C—OH groups in glucose and citrate, O— containing groups on the HOPG surface and adventitious contaminations (C 1s spectra are not given in figures). Oxygen species interacting with Ag, in particular, OH chemisorbed on Ag (531.2 eV), electrophilic $O^{\delta-}$ atoms (denoted as Oβ) dissolved in Ag^0 lattice (~530.8 eV) or localized on the metal surface (~530.5 eV) [10–14,17,18,49] are observable at lower BE, but to resolve the signals unambiguously is difficult. These O species cause no shift of Ag peaks, allowing to discriminate them from oxygen in silver carbonate that has been found on silver surfaces at low temperatures [14,17,18,49] but seems to be negligible here. Signals near 529.6 eV attributable to nucleophilic O bonded to Ag(I) atoms in a silver oxide (designated as Oα) [14,17–19,21,49,57] are very weak, if any. The ratios of surface OH— group and electrophilic oxygen Oβ to Ag are in the range 0.19–0.5 (Supplementary data, Table 1), in reasonable agreement with those reported for Ag crystal electrode contacted with aqueous solutions [17–19,21] and Ag NPs exposed to gas phase oxygen [14,49]; the values are lower for capped nanoparticles and for smaller ones due to the presence of capping agents and uptaken water. The exposure of the larger Ag NPs at atmosphere for several days entails a slow increase in the width of Ag 3d and Ag MNN bands, while the changes in the O 1s spectra of smaller silver clusters are less straightforward owing to complex transformations of surface Ag—O species [14]. Furthermore, XPS analysis revealed chloride and, in some cases, sulfide

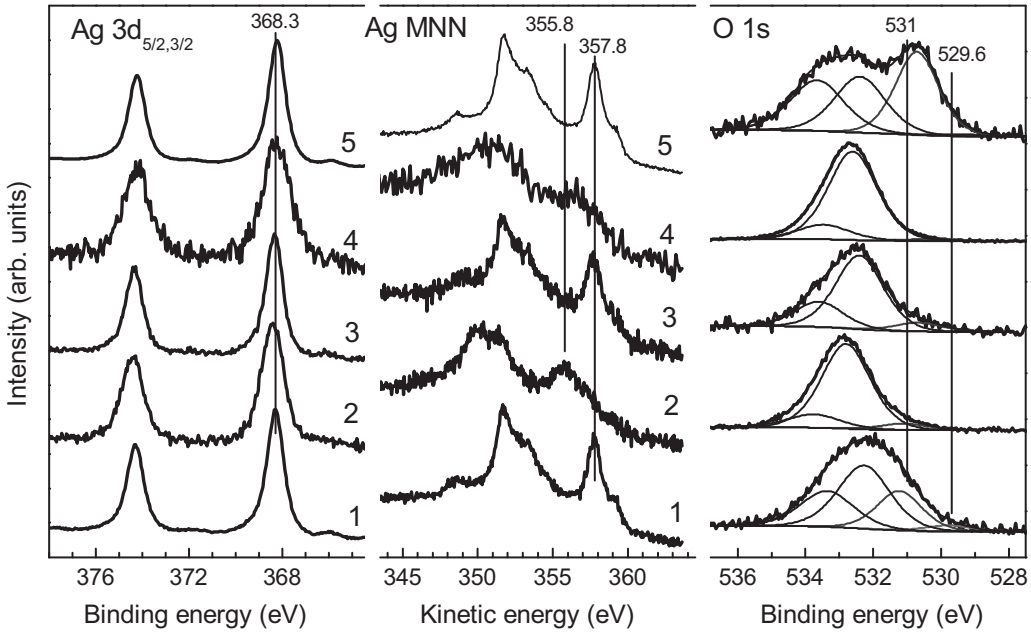

Fig. 5. X-ray photoelectron spectra normalized to height from silver NPs prepared with (1) $AgNO_3/NaBH_4$ = 1, (2) $AgNO_3/NaBH_4$ = 10, (3) $AgNO_3/Na_3cit/NaBH_4$, (4) $AgNO_3$/glucose, and deposited on HOPG.

species uptaken from the laboratory atmosphere, more readily by the smaller Ag NPs produced both via borohydride- and glucose-assisted synthesis. The atomic ratio Ag to Cl plus S may reach 0.1–0.2, so these contaminations also contribute to broadening of the Ag spectra. In brief summary, a measure of oxidation of Ag NPs is relatively low for 10–15 nm Ag NPs, both uncapped and citrate-protected; it is larger for the uncapped Ag NPs manufactured with $AgNO_3/NaBH_4 = 10$ (this also confirms that 2–5 nm NPs do determine the surface characteristics of this product) and for those prepared in the glucose-assisted synthesis, with the oxidized silver representing mobilized or adsorbed Ag^+ species rather than Ag(I) oxide.

3.3. Electrochemical oxidation of supported Ag NPs

3.3.1. Cyclic voltammetry

Cyclic voltammograms for the four types of Ag NPs deposited on HOPG and for polished polycrystalline Ag plate acquired in 1 M NaOH are shown in Fig. 6. The anodic maxima referred as A1–A3 and A4 in the CVA of bulk Ag electrode coincide with those reported in the literature and associated with the formation of Ag_2O and AgO ($Ag^+Ag^{3+}O_{2-x}$) via net reactions

$$2Ag + 2OH^- = Ag_2O + H_2O + 2e$$

and

$$Ag_2O + 2OH^- = 2AgO + H_2O + 2e,$$

respectively; the cathodic peaks C1 and C2 are due to the reverse reactions. The electrochemical oxidation of Ag to Ag_2O involves at least three stages corresponding to the A1, A2 and A3 features, which are most often ascribed to (i) the formation of a monolayer of Ag_2O or AgOH, or/and dissolution of Ag species, (ii) the formation of a Ag_2O base layer ("primary" oxide, possibly hydrated), and (iii) the nucleation and 3D growth of crystalline Ag_2O phase ("secondary" oxide), respectively [15–18,20]. The evolution of oxygen contributes to the anodic current at the potentials above ~0.8 V.

The anodic oxidation of the uncapped ~12 nm Ag NPs (curve b) starts at lower potentials than that of bulk silver, but the anodic maximum A3 is almost absent, indicating that the 3D Ag_2O does not crystallize upon the sweep. The narrow peak A4 corresponding to nucleation and growth of AgO at the expense of Ag_2O [16,19,21] is also shifted towards a less positive potential, probably because the nucleation proceeds easier on the poorly ordered "primary" Ag_2O. The smaller uncapped Ag NPs prepared with $AgNO_3/NaBH_4 = 10$ oxidize to Ag_2O at more positive potentials (but at lesser ones than Ag plate), and the preliminary maxima A1–A2 at 0.2–0.3 V are relatively low. This can be explained by the surface oxidation of the Ag NPs prior the potential sweep (see XPS data above). Strictly speaking, the current magnitudes for different Ag NP samples cannot be directly compared because of various surface areas. In particular, we failed to normalize reliably the current using Ag concentrations derived from XPS, largely due to various thickness of protecting molecule or/and hydrous shells above the silver cores. Nevertheless, we assert that the peak A3 and the charge passed in the anodic formation of Ag_2O are larger for the small unprotected Ag NPs in comparison with the bigger ones, and this is confirmed by XPS data below. The peak A4 is wide and occurs at higher overpotentials; this, along with lesser cathodic C2 maximum, shows that the formation of AgO is impeded. For citrate- and glucose-capped Ag NPs, the anodic maxima A1–A3 and A4 are essentially broadened and shifted to more positive potentials, and the currents are lower than for the uncapped particles, implying that all the reactions are notably retarded.

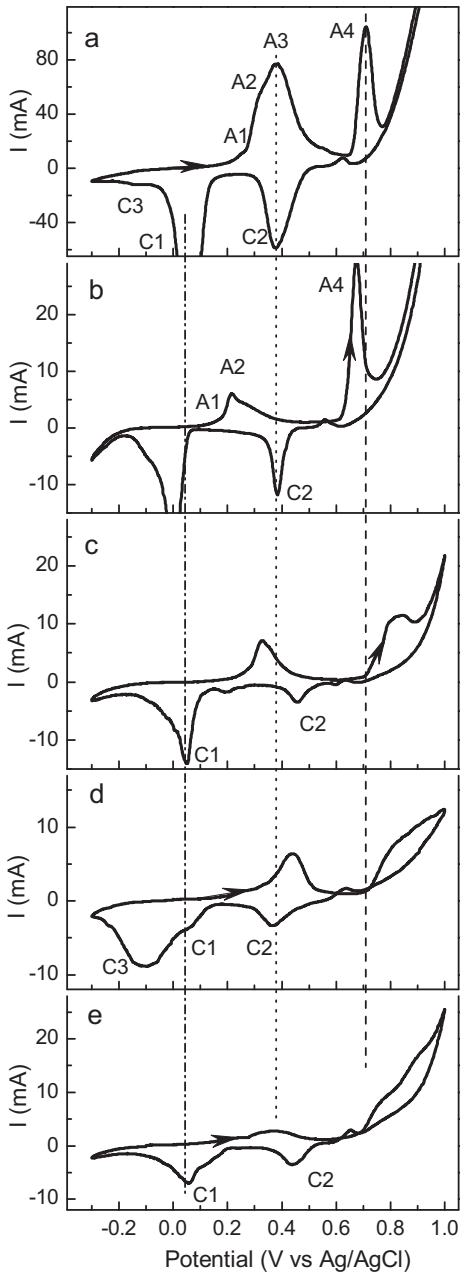

Fig. 6. Cyclic voltammograms of (a) polycrystalline Ag plate and HOPG with Ag NPs deposited from their hydrosols prepared with (b) $AgNO_3/NaBH_4 = 1$, (c) $AgNO_3/NaBH_4 = 10$, (d) $AgNO_3/Na_3cit/NaBH_4$, (e) $AgNO_3$/glucose, in 1 M NaOH. The voltammograms (sweep rate 5 mV/s) were initiated in positive-going direction from stationary potentials near 0.1 V.

There also are differences in the position and shape of cathodic maxima for bulk metal and various Ag NPs. The reduction of AgO to Ag_2O (peak C2) proceeds at more positive potentials (430–450 mV vs Ag/AgCl), that is easier for the smaller Ag NPs, both uncapped and capped, than for the larger ones and metal plate. On the other hand, instead of a single major peak C1 for the bulk electrode, the Ag NPs exhibit two or three maxima. The main peak corresponding to the reduction of 3D Ag_2O [15,16] is situated at +0.05 V for bulk electrode and for the two sorts of tiny, 3–5 nm Ag NPs, while it is centered at about 0 V for larger uncapped Ag NPs (prepared with $AgNO_3/NaBH_4 = 1$). A feature near −0.1 V attributable to the reduction of hydrous Ag(I) oxide [15] is enhanced for nanosilver, being largest for citrate-capped nanoparticles. This suggests that a Ag(I) oxide formed on these Ag NPs is notably disordered. A minor

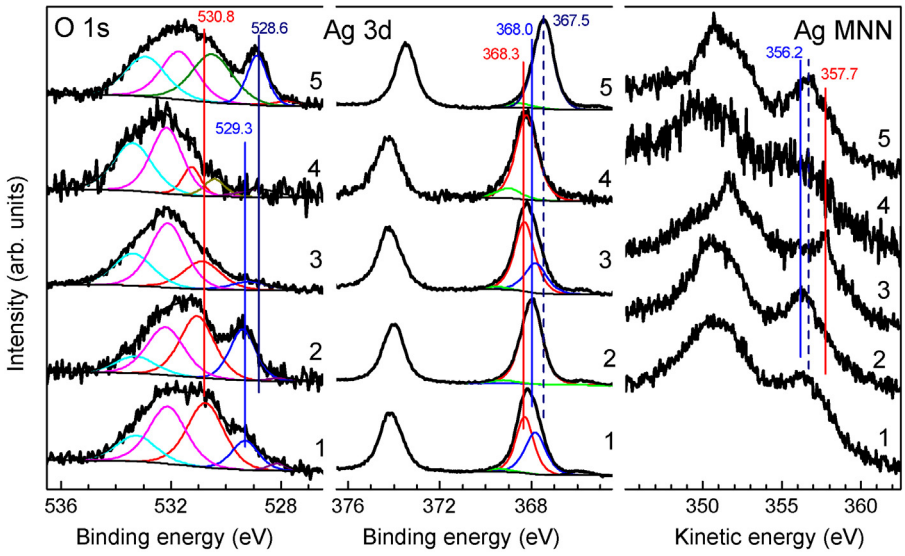

Fig. 7. X-ray photoelectron spectra (normalized to height) from silver NPs prepared with $AgNO_3/NaBH_4 = 1$ (1), $AgNO_3/NaBH_4 = 10$ (2), $AgNO_3/Na_3cit/NaBH_4$ (3), $AgNO_3$/glucose(4) and polycrystalline Ag plate (5) oxidized in the potential sweep to +0.7 V (5 mV/s) in 1 M NaOH.

cathodic maximum at 0.12–0.18 V seen at the cathodic curves of the 3–5 nm Ag NPs, both uncapped and glucose-capped, is likely due to the reduction of solubilized Ag(I) species [15].

3.3.2. XPS analysis

The differences in the oxidation products are most evident for the samples polarized in the sweep to +0.7 V (Fig. 7 and Supplementary data, Table 2). The intensity at 531–530 eV originating from surface OH groups or/and electrophilic oxygen Oβ increases considerably; separation of these signals by deconvolution of the spectra is not unique, and it is not shown here. An exception is the spectrum of glucose-capped Ag NPs, where the lines of OH groups at 531.2 eV and, probably, surface localized Oβ at 530.3 eV can be clearly resolved. The signals from nucleophilic oxygen Oα bonded to Ag in Ag_2O and AgO can be seen at the binding energy decreasing in the range 529.5–528.6 eV with an increase in the contents of oxygen and Ag^{3+} in the AgO_{1-x} products [21]. There is also a weak band at 528.2 eV that has been proposed to attribute to 2D Ag(I) oxide [17,18].

The Ag 3d lines broaden and shift to lower binding energies due to the formation of silver oxides. The Ag $3d_{5/2}$ maximum of oxidized polycrystalline Ag plate is centered at the BE as low as 367.5 eV, indicating that the surface layer is preferentially composed of AgO_{1-x} oxide, in agreement with the position of the relevant O 1s line at 528.6 eV and the Ag $M_5N_4N_4$ maximum at 356.7 eV [19,21,57]. The oxidation of the unprotected small Ag NPs (spectra 2 in Fig. 7) leads to a comparably narrow Ag $3d_{5/2}$ maximum at 368.0 eV, the Ag $M_5N_4N_4$ kinetic energy of 356.3 eV, and the O 1s signal at 529.4 eV, evidencing that Ag(I) oxide is the main product, whereas contributions from Ag(0) and Ag(II) oxide are negligible. This implies almost complete oxidation of the 3–5 nm Ag NPs to crystalline 3D Ag_2O, in concurrence with the results of cyclic voltammetry.

The spectra of other three samples are broader due to contributions from several substances. For larger Ag NPs, both uncapped and citrate-capped, the Ag $3d_{5/2}$ bands are better fitted with two major peaks at 368.3 eV and 367.8 eV corresponding to Ag metal and Ag(I) oxide. The quantity of the oxide phase is higher for the uncapped particles but it is obviously lower than for the smaller "naked" Ag NPs, again in concordance with the electrochemical data. The Ag 3d and respective O 1s features are slightly shifted to lower BE, but there are no unequivocal spectroscopic evidences for AgO_{1-x}, the formation of which is expected from the voltammetry (peak A4). In all likelihood, the quantity of Ag^{3+} species is small and that readily reduces under open-circuit conditions and X-ray beam [21]. The spectra of the oxidized glucose-capped small Ag NPs contain signals from Ag metal, minor Ag(I) oxide, and a Ag 3d line at 369 eV, which likely originates from ionic Ag^+ species, for example, hydrous AgOH and Ag^+-glucose complexes, or very small Ag^0 clusters exhibiting the final state effect owing to a photohole in the core level [57,58].

3.4. On the effect of capping and size on the reactivity of Ag NPs

The results show clear and well reproducible influence of size and capping of nanoparticles on their behavior. One can see that citrate ions and glucose molecules impede anodic oxidation of Ag NPs both to Ag_2O and AgO, but they do not perfectly protect the Ag NPs against gradual oxidation at open-circuit potentials. At the same time, the photoelectron and Auger spectra show that near-surface concentrations of Ag(I) species for the capped Ag NPs are higher than for uncapped ones of approximately the same diameter. The broad maxima in the voltammetric curves also suggest that hydrated silver (I) oxide and some mobile or adsorbed Ag(I) species are more strongly involved in redox reactions of the capped nanoparticles. On the other hand, certain similarities are observed for the cyclic voltammograms of the uncapped and capped NPs of about the same size (Fig. 6).

The effect of particle size on the reactivity is not quite straightforward. The smaller Ag NPs more easily enter into oxidation-reduction reactions, and the resistive switching being observed in the tunneling spectra of the "naked" particles. Interestingly, the anodic oxidation of the smaller uncoated Ag NPs yields 3D Ag_2O (peak A3 in Fig. 6), similar to bulk Ag electrode, whereas the oxidation of larger nanoparticles is limited by a layer of "primary" Ag(I) oxide. Nucleation of Ag(II) oxide (peak A4) appears to proceed readily on the defective oxide formed, while it is retarded on 3D Ag_2O (that is, at smaller uncoated particles) and protected Ag NPs. However, a much thicker layer of AgO_{1-x} grows under the same conditions at silver plate. It should be noted that, despite the supported nanoparticles are partially aggregated, the internally

consistent description of their behavior can be achieved utilizing the dimensions of individual Ag NPs derived from SAXS and TEM and, in part, STM. This and high reproducibility of the results imply that the aggregation (at least, at low surface coverage) and possible collateral effects do not play a significant role.

We hesitate to draw far-reaching conclusions about mechanisms behind these phenomena, especially as there remain, after decades of research, many open questions about the mechanism of bulk silver oxidation [15–21]. It can be suggested at the moment that the capping molecules facilitate oxidation and solubilization of surface Ag atoms but slow down diffusion of the mobilized Ag species and their release into the environment. Furthermore, the organic capping probably inhibits the formation of electrophilic atomic oxygen (Oβ), incorporation of which into Ag lattice seems to be a necessary pre-oxidation stage [17,18]; some hints for this are provided by the photoelectron spectra. The inhibition could be caused by reactions of transient oxygen species with the organic molecules and/or by binding of OH groups (a precursor for Oβ) by Ag^+ ions entrapped within the shells. On the other hand, near-surface concentrations of mobile Ag species are less due to lower surface area of 10–12 nm particles as compared with the 3–5 nm NPs and bulk metal, when the Ag NPs, even somewhat aggregated, do not form a continuous film; more perfect structure of the larger particles may play a role too. As a result, the crystallization of 3D Ag_2O that is thought to require a release of intermediary soluble Ag(I) species [15] is effectively suppressed on the larger Ag NPs. In fact, the ability to mobilize transient Ag species emerges as a key factor determining the specific reactivity of silver nanoparticles.

4. Conclusions

Silver nanoparticles of 10–12 nm particles without and with citrate capping and about 3–5 nm Ag NPs, either uncapped or glucose-capped, were synthesized, and the electrochemical reactions of the nanoparticles deposited on HOPG were examined using tunneling spectroscopy setup, XPS, cyclic voltammetry. A resistive switching effect was observed for the uncapped 3–5 nm Ag NPs in tunneling spectra measured in air; it was rationalized in terms of transfer of Ag species between the nanoparticle and the probe, shortening the distance or making nanoscale contacts. The anodic oxidation of uncapped Ag NPs started at lower potentials than bulk silver electrode but the smaller Ag NPs, similar to the Ag plate, yielded "secondary" 3D Ag_2O, whereas the oxidation of larger nanoparticles produced only a layer of "primary" Ag(I) oxide. The following formation of AgO at higher potentials proceeded readily at the defective oxide at about 12 nm particles while it was retarded at the smaller ones. The citrate ions and glucose molecules capping Ag NPs substantially impeded both the formation of Ag_2O and the nucleation of AgO during the anodic sweep, but they poorly protected the Ag NPs against slower oxidation in air. The results underline importance of the intermediate mobilization of Ag species, which depends upon the size and capping of silver nanoparticles, for the reaction mechanisms.

Acknowledgements

This work was partially financially supported by the Ministry of Education and Science of RF (Grant 8580) and RFBR (12-03-31178).

Appendix A. Supplementary data

Supplementary material related to this article can be found, in the online version, at http://dx.doi.org/10.1016/j.apsusc.2014.01.081.

References

[1] Y.A. Krutyakov, A.A. Kudrinskiy, A.Y. Olenin, G.V. Lisichkin, Synthesis and properties of silver nanoparticles: advances and prospects, Russ. Chem. Rev. 77 (2008) 233–257.
[2] B. Sepulveda, P.C. Angelome, L.M. Lechuga, L.M. Liz-Marzan, LSPR-based nanobiosensors, Nano Today 4 (2009) 244–251.
[3] M. Rai, A. Yadav, A. Gade, Silver nanoparticles as a new generation of antimicrobials, Biotechnol. Adv. 27 (2009) 76–83.
[4] Y.M. Li, G.A. Somorjai, Nanoscale advances in catalysis and energy applications, Nano Lett. 10 (2010) 2289–2295.
[5] H.A. Atwater, A. Polman, Plasmonics for improved photovoltaic devices, Nat. Mater. 9 (2010) 205–213.
[6] J. Fabrega, S.N. Luoma, C.R. Tyler, T.S. Galloway, J.R. Lead, Silver nanoparticles: behaviour and effects in the aquatic environment, Environ. Int. 37 (2011) 517–531.
[7] C. Levard, E.M. Hotze, G.V. Lowry, G.E. Brown Jr., Environmental transformations of silver nanoparticles: impact on stability and toxicity, Environ. Sci. Technol. 46 (2012) 6900–6914.
[8] J. Liu, Z. Wang, F.D. Liu, A.B. Kane, R.H. Hurt, Chemical transformations of nanosilver in biological environments, ACS Nano 6 (2012) 9887–9899.
[9] D.J. De Aberasturi, V. Wulf, B. Pelaz, P. Del Pino, Y. Zhao, J.M. De La Fuente, I.R. De Larramendi, T. Rojo, X.-J. Liang, W.J. Parak, The challenge to relate the physicochemical properties of colloidal nanoparticles to their cytotoxicity, Acc. Chem. Res. 46 (2013) 743–749.
[10] C. Rehren, G. Isaac, R. Schlögl, G. Ertl, Surface and subsurface products of the interaction of O_2 with Ag under catalytic conditions, Catal. Lett. 11 (1991) 253–265.
[11] V.I. Bukhtiyarov, A.F. Carley, L.A. Dollard, M.W. Roberts, XPS study of oxygen adsorption on supported silver: effect of particle size, Surf. Sci. 381 (1997) L605–L608.
[12] V.I. Bukhtiyarov, V.V. Kaichev, The combined application of XPS and TPD to study of oxygen adsorption on graphite-supported silver clusters, J. Mol. Catal. A 158 (2000) 167–172.
[13] L.S. Kibis, A.I. Stadnichenko, E.M. Pajetnov, S.V. Koscheev, V.I. Zaykovskii, A.I. Boronin, The investigation of oxidized silver nanoparticles prepared by thermal evaporation and radio-frequency sputtering of metallic silver under oxygen, Appl. Surf. Sci. 257 (2010) 404–413.
[14] T.C.R. Rocha, A. Oestereich, D.V. Demidov, M. Hävecker, S. Zafeiratos, G. Weinberg, V.I. Bukhtiyarov, A. Knop-Gericke, R. Schlögl, The silver–oxygen system in catalysis: new insights by near ambient pressure X-ray photoelectron spectroscopy, Phys. Chem. Chem. Phys. 14 (2012) 4554–4564.
[15] L. Teijelo, J.R. Vilche, A.J. Arvia, Comparative voltammetric behaviour of the silver/silver oxide electrode prepared on vitreous carbon and silver substrates, J. Appl. Electrochem. 18 (1988) 691–698.
[16] T.U. Hur, W.S. Chung, The mechanism of silver(I) oxide to silver(II) oxide formation on polycrystalline silver electrodes in 8 M KOH solution, J. Electrochem. Soc. 152 (2005) A996–A1000.
[17] E.R. Savinova, D. Zemlyanov, B. Pettinger, A. Scheybal, R. Schlögl, K. Doblhofer, On the mechanism of Ag(1 1 1) sub-monolayer oxidation: a combined electrochemical, in situ SERS and ex situ XPS study, Electrochim. Acta 46 (2000) 175–183.
[18] E.R. Savinova, A. Scheybal, M. Danckwerts, U. Wild, B. Pettinger, K. Doblhofer, R. Schlögl, G. Ertl, Structure and dynamics of the interface between a Ag single crystal electrode and an aqueous electrolyte, Faraday Discuss. 121 (2002) 181–198.
[19] D. Lützenkirchen-Hecht, H.-H. Strehblow, The anodic oxidation of silver in 1 M NaOH: electrochemistry, ex situ XPS and in situ X-ray absorption spectroscopy, Surf. Interf. Anal. 38 (2006) 686–690.
[20] V. Maurice, L.H. Klein, H.-H. Strehblow, P. Marcus, In situ STM study of the surface structure, dissolution, and early stages of electrochemical oxidation of the Ag(1 1 1) electrode, J. Phys. Chem. C 111 (2007) 16351–16361.
[21] D. Lützenkirchen-Hecht, H.-H. Strehblow, Anodic silver (II) oxides investigated by combined electrochemistry, ex situ XPS and in situ X-ray absorption spectroscopy, Surf. Interf. Anal. 41 (2009) 820–829.
[22] R.W. Murray, Nanoelectrochemistry: metal nanoparticles, nanoelectrodes, and nanopores, Chem. Rev. 108 (2008) 2688–2720.
[23] L. Tang, X. Li, R.C. Cammarata, C. Friesen, K. Sieradzki, Electrochemical stability of elemental metal nanoparticles, J. Am. Chem. Soc. 132 (2010) 11722–11726.
[24] K.H. Ng, H. Liu, R.M. Penner, Subnanometer silver clusters exhibiting unexpected electrochemical metastability on graphite, Langmuir 16 (2000) 4016–4023.
[25] O.S. Ivanova, F.P. Zamborini, Size-dependent electrochemical oxidation of silver nanoparticles, J. Am. Chem. Soc. 132 (2010) 70–72.
[26] P. Singh, K.L. Parent, D.A. Buttry, Electrochemical solid-state phase transformations of silver nanoparticles, J. Am. Chem. Soc. 134 (2012) 5610–5617.
[27] P. Singh, D.A. Buttry, Comparison of oxygen reduction reaction at silver nanoparticles and polycrystalline silver electrodes in alkaline solution, J. Phys. Chem. C 116 (2012) 10656–10663.
[28] O.V. Dement'eva, A.V. Mal'kovskii, M.A. Filippenko, V.M. Rudoy, Comparative study of the properties of silver hydrosols prepared by citrate and citrate–sulfate procedures, Colloid J. 70 (2008) 561–573.
[29] J.Y. Liu, R.H. Hurt, Ion release kinetics and particle persistence in aqueous nanosilver colloids, Environ. Sci. Technol. 44 (2010) 2169–2175.
[30] J. Liu, K.G. Pennell, R.H. Hurt, Kinetics and mechanisms of nanosilver oxysulfidation, Environ. Sci. Technol. 45 (2011) 7345–7353.

[31] X. Li, J.J. Lenhart, H.W. Walker, Aggregation kinetics and dissolution of coated silver nanoparticles, Langmuir 28 (2012) 1095–1104.
[32] Y. Han, R. Lupitskyy, T.-M. Chou, C.M. Stafford, H. Du, S. Sukhishvili, Effect of oxidation on surface-enhanced Raman scattering activity of silver nanoparticles: a quantitative correlation, Anal. Chem. 83 (2011) 5873–5880.
[33] X.C. Jiang, A.B. Yu, Silver nanoplates a highly sensitive material toward inorganic anions, Langmuir 24 (2008) 4300–4309.
[34] E.A. Vishnyakova, S.V. Saikova, R.B. Nikolaeva, Y.L. Mikhlin, Synthesis of anisotropic silver nanoparticles and investigation of their sensory properties, Russ. J. Inorg. Chem. 57 (2012) 152–159.
[35] K.C. Nguyen, V.L. Seligy, A. Massarsky, T.W. Moon, P. Rippstein, J. Tan, A.F. Tayabali, Comparison of toxicity of uncoated and coated silver nanoparticles, J. Phys. Conf. Ser. 429 (2013) 012025.
[36] Z. Xiu, Q. Zhang, H.L. Puppala, V.L. Colvin, P.J.J. Alvarez, Negligible particle-specific antibacterial activity of silver nanoparticles, Nano Lett. 12 (2012) 4271–4275.
[37] D. He, S. Garg, T.D. Waite, H_2O_2-mediated oxidation of zero-valent silver and resultant interactions among silver nanoparticles, silver ions, and reactive oxygen species, Langmuir 28 (2012) 10266–10275.
[38] R. Ma, C. Levard, S.M. Marinakos, Y. Cheng, J. Liu, F.M. Michel, G.E. Brown Jr., G.V. Lowry, Size-controlled dissolution of organic-coated silver nanoparticles, Environ. Sci. Technol. 46 (2012) 752–759.
[39] G.A. Sotiriou, A. Meyer, J.T.N. Knijnenburg, S. Panke, S.E. Pratsinis, Quantifying the origin of released Ag^+ ions from nanosilver, Langmuir 28 (2012) 15929–15936.
[40] R.D. Glover, J.M. Miller, J.E. Hutchison, Generation of metal nanoparticles from silver and copper objects: nanoparticle dynamics on surfaces and potential sources of nanoparticles in the environment, ACS Nano 5 (2011) 8950–8957.
[41] S. Wojtysiak, A. Kudelski, Influence of oxygen on the process of formation of silver nanoparticles during citrate/borohydride synthesis of silver sols, Colloid Surf. A 410 (2012) 45–51.
[42] B.M. Sergeev, L.I. Lopatina, G.B. Sergeev, The influence of Ag^+ ions on transformations of silver clusters in polyacrylate aqueous solutions, Colloid J. 68 (2006) 761–766.
[43] D.L. Van Hyning, C.F. Zukoski, Formation mechanisms and aggregation behavior of borohydride reduced silver particles, Langmuir 14 (1998) 7034–7046.
[44] X. Zou, E. Ying, H. Chen, S. Dong, An approach for synthesizing nanometer- to micrometer-sized silver nanoplates, Colloid Surf. A 303 (2007) 226–234.
[45] D.I. Svergun, Determination of the regularization parameter in indirect-transform methods using perceptual criteria, J. Appl. Crystallogr. 25 (1992) 495–503.
[46] H. Hövel, T. Becker, A. Bettac, B. Reihl, M. Tschudy, E.J. Williams, Controlled cluster condensation into preformed nanometer-sized pits, J. Appl. Phys. 81 (1997) 154–158.
[47] I. Lopez-Salido, D.C. Lim, Y.D. Kim, Ag nanoparticles on highly ordered pyrolytic graphite (HOPG) surfaces studied using STM and XPS, Surf. Sci. 588 (2005) 6–18.
[48] S.H. Jeong, D.C. Lim, J.-H. Boo, S.B. Lee, H.N. Hwang, C.C. Hwang, Y.D. Kim, Interaction of silver with oxygen on sputtered pyrolytic graphite, Appl. Catal. A: Gen. 320 (2007) 152–158.
[49] D.V. Demidov, I.P. Prosvirin, A.M. Sorokin, V.I. Bukhtiyarov, Model Ag/HOPG catalysts: preparation and STM/XPS study, Catal. Sci. Technol. 1 (2011) 1432–1439.
[50] R. Waser, M. Aono, Nanoionics-based resistive switching memories, Nat. Mater. 6 (2007) 833–840.
[51] A. Sawa, Resistive switching in transition metal oxides, Mater. Today 11 (2008) 28–33.
[52] J.-S. Lee, Progress in non-volatile memory devices based on nanostructured materials and nanofabrication, J. Mater. Chem. 21 (2011) 14097–14112.
[53] L.L. Wei, J. Wang, Y.S. Chen, D.S. Shang, Z.G. Sun, B.G. Shen, J.R. Sun, Pulse-induced alternation from bipolar resistive switching to unipolar resistive switching in the $Ag/AgO_x/Mg_{0.2}Zn_{0.8}O/Pt$ device, J. Phys. D: Appl. Phys. 45 (2012) 425303.
[54] Y. Naitoh, S. Takeshita, D. Ishida, E. Ohmura, K. Kobayashi, H. Yamada, Y. Majima, Resistive switching effects in metallic nanogap electrode fabricated by electroless gold plating, Appl. Phys. Express 5 (2012) 085201.
[55] A. Kiazadeh, H.L. Gomes, A.M.R. da Costa, J.A. Moreira, D.M. de Leeuw, S.C.J. Meskers, Intrinsic and extrinsic resistive switching in a planar diode based on silver oxide nanoparticles, Thin Solid Films 522 (2012) 407–411.
[56] S. Tanuma, C.J. Powell, D.R. Penn, Calculations of electron inelasticmean free paths. IX. Data for 41 elemental solids over the 50 eV to 30 keV range, Surf. Interf. Anal. 43 (2011) 689–713.
[57] A.M. Ferraria, A.P. Carapeto, A.M.B. do Rego, X-ray photoelectron spectroscopy: silver salts revisited, Vacuum 86 (2012) 1988–1991.
[58] A. Tanaka, Y. Takeda, T. Nagasawa, S. Sato, Dynamic final-state nanoparticle–substrate in the photoemission of dodecanethiolate-passivated Ag nanoparticles on graphite substrates, Phys. Rev. B 67 (2003) 033101.